The Astrophysical Journal, 606:555–564, 2004 May 1

ABUNDANCES OF HEAVY AND ULTRAHEAVY IONS IN ^{3}He-RICH SOLAR FLARES

G. M. Mason,[1,2] J. E. Mazur,[3] J. R. Dwyer,[4] J. R. Jokipii,[5] R. E. Gold,[6] and S. M. Krimigis[6]

Received 2003 September 30; accepted 2004 January 9

ABSTRACT

We have surveyed ^{3}He-rich solar energetic particle (SEP) events over the period 1997 September–2003 April in order to characterize abundances of heavy ions near 400 keV nucleon^{-1}. The first part of the study focuses on 20 distinct SEP events that show the previously observed pattern in which, relative to O, heavy ions through Fe are enriched, with the enrichment increasing with mass. We find that these enrichments are well correlated such that ^{3}He-rich SEP events with high Fe/C also show larger enrichments in other heavy ions. Ultraheavy (UH; taken as 78–220 amu) ions are routinely seen in these events with abundance enhancements correlating with Fe/C but with even larger flare-to-flare variations. In one event with unusually little interplanetary scattering, we are able to estimate the time of heavy- and UH-ion injections at the Sun and find them to be simultaneous. The second part of the study sums up many impulsive-event time periods in order to construct a mass histogram of UH nuclei; this histogram shows broad mass peaks similar to those in compilations of solar system abundances. In this summed period, relative to O, the average enhancement of heavy nuclei increases with mass with values of $\sim$7 for Fe, $\sim$40 for mass 78–100 amu, $\sim$120 for mass 125–150 amu, and $\sim$215 for 180–220 amu. The maximum UH enhancements seen in the most-enriched events are at least a factor of 5 larger. The enhancements are approximately proportional to the particle charge-to-mass ratio raised to a power, as seen previously in large, shock-associated SEP events.

Subject headings: acceleration of particles — cosmic rays — shock waves — solar wind — Sun: abundances — Sun: flares

1. INTRODUCTION

Solar energetic particle (SEP) events with large enrichments of the rare isotope ^{3}He (up to factors of 10^5) have long been known to be associated with large enhancements (factor of 3–10) of heavy-ion ratios such as Ne/O and Fe/O, compared to large-SEP events. In addition, compared to large-SEP events, ^{3}He-rich events are generally short lasting, are associated with type III electron bursts, and exhibit significantly higher heavy-ion charge states. Many theoretical studies have been undertaken to model these particle events, generally making use of the unique charge-to-mass (Q/M) ratio of ^{3}He and the difference between the Q/M ratio of heavier ions and that of oxygen expected at coronal temperatures (e.g., see reviews by Kocharov & Kocharov 1984; Miller 1998; Reames 1999). This research remains quite active, with a number of possible mechanisms still being studied.

Recently, Reames (2000) reported very large enhancements of trans-iron elements relative to O in several impulsive solar particle events, with $34 \leq Z \leq 40$ and $50 \leq Z \leq 56$ enhanced by factors of $\sim$100 and $\sim$1000, respectively, over the coronal values (see also Price et al. 1973; Shirk & Price 1973). Compared to Fe, which is already enhanced by a factor of $\sim$10 in these events, these UH nuclei ($\equiv$78–220 amu) were therefore showing additional enhancement factors of $\sim$10 and $\sim$100. Even with these large enhancements, the extreme rarity of these UH nuclei can be appreciated from the fact that the Reames (2000) $\sim$5.5 yr survey listed only nine impulsive-SEP events showing a few counts of trans-iron nuclei each, even though during this period ^{3}He from impulsive-SEP events was present in the interplanetary medium on the majority of days (Wiedenbeck et al. 2003b).

In order to explore these issues further, we have carried out a multiyear survey of ^{3}He-rich SEP events using an instrument with an energy threshold more than an order of magnitude lower than the Reames (2000) survey, thereby allowing greatly improved statistical precision because of the steep energy spectra. We have focused on ^{3}He events whose intensity, although small compared to large-SEP events, was large enough to minimize statistical uncertainties. The main findings of our study are as follows:

1. In the range C–Fe, the enrichments of the ions are all positively correlated, with mean values similar to previous studies.
2. UH nuclei (mass 78–220 amu) are present in dozens of impulsive events with enhancements of up to hundreds of times the Fe enhancement.
3. In one event with unusually low scattering during transport to 1 AU, the heavy nuclei through Fe were accelerated within a few minutes of the associated flare X-ray burst, and the UH nuclei appeared (with greater uncertainties) to be simultaneously accelerated.
4. The abundance enhancement pattern and correlations observed for the elements up to Fe, and for mass groupings above that (78–100, 125–150, and 180–220 amu), can be reasonably fitted by a power law in particle Q/M ratio for a $\sim$3 MK plasma, as observed previously in large-SEP events

[1] Department of Physics, University of Maryland, College Park, MD 20742; glenn.mason@umail.umd.edu.
[2] Institute for Physical Science and Technology, University of Maryland, College Park, MD 20742.
[3] Aerospace Corporation, 2350 East El Segundo Boulevard, El Segundo, CA 90245-4691.
[4] Department of Physics and Space Sciences, Florida Institute of Technology, Melbourne, FL 32901.
[5] Department of Planetary Sciences, Lunar and Planetary Laboratory, University of Arizona, Tucson, AZ 85721.
[6] Johns Hopkins University Applied Physics Laboratory, Laurel, MD 20723.

(Breneman 1985; Breneman & Stone 1985; Cohen et al. 1999; Leske et al. 1999; Dwyer et al. 2001).

2. OBSERVATIONS

2.1. *Instrumentation*

Our observations were carried out with the Ultra Low Energy Isotope Spectrometer (ULEIS; Mason et al. 1998), which was launched on the *Advanced Composition Explorer* (*ACE*) spacecraft in 1997 August (Stone et al. 1998). ULEIS is a time-of-flight (TOF) mass spectrometer that identifies particle mass by measuring the TOF t over a $\sim$0.5 m path and the energy E deposited in an array of solid state detectors. Particles enter the telescope through thin foils that emit secondary electrons that are deflected onto microchannel plates to produce "start" signals for timing. When particles penetrate a foil just in front of the solid state detector, they emit secondary electrons used for a "stop" signal and also deposit their residual kinetic energy in the detector. Since the kinetic energy $E = \frac{1}{2}mv^2$, the particle mass and incident energy can be obtained after correcting for energy losses in the telescope foils and detector windows. Note that the particle atomic number Z is not measured. The start and stop microchannel plates use "wedge-strip-zigzag" anodes that are pulse-height analyzed in order to identify the location on the foil where the ion passes (for details see Mason et al. 1998). Because of the long path length, precise timing measurement, measurement of the particle trajectory in the instrument, and low background, ULEIS has excellent mass resolution; for example, it is able to resolve ^{3}He from ^{4}He at abundance ratios of less than 0.5% (e.g., see Mason, Mazur, & Dwyer 1999).

Since the UH nuclei are extremely rare and individual mass peaks are not separated, it is not possible to use in-flight data to verify the instrument response in the range above Fe. We therefore calibrated an engineering unit of ULEIS whose telescope and front-end electronics were identical to the flight unit. The calibration was done at the Brookhaven National Laboratory tandem Van de Graaff accelerator. Figure 1 shows calibration mass peaks of selected ions for energies of less than 0.5 MeV nucleon^{-1}, which are typical for the flight observations discussed below. The peak widths appear approximately the same width on the logarithmic scale, and thus the mass resolution σ_m/m is approximately constant, as expected. A typical value from the figure is $\sigma_m/m = 0.040$, so for example, at Au, $\sigma_m = 7.9$ amu. Since many mass peaks are simultaneously present in the flight data, individual mass peaks there will overlap. After examining the engineering model instrument response to heavy ions, we found that we required only small adjustments to the flight unit calibration to extend it to the UH region.

Background is an important consideration in the UH region because of the extremely low fluxes and the fact that individual mass peaks are not resolved. Two critical features of the ULEIS design made it possible to assess background issues in the flight data: dual measurements of the TOF in the telescope, and measurement of the ion trajectory that returned information on the number of secondary electrons emitted as the ions traversed the telescope foils. Thus, for each heavy ion there were many separate measurements transmitted, allowing for consistency checks that made it possible to eliminate background. Unfortunately, in 2000 April after about 2.5 yr of operation, the microchannel-plate stack used for the first TOF start signal suddenly lost most of its gain, rendering this TOF useless. However, the UH data collected up to this point made it possible to assess the background issues when operating with a single TOF in order to extend our survey beyond 2000 April.

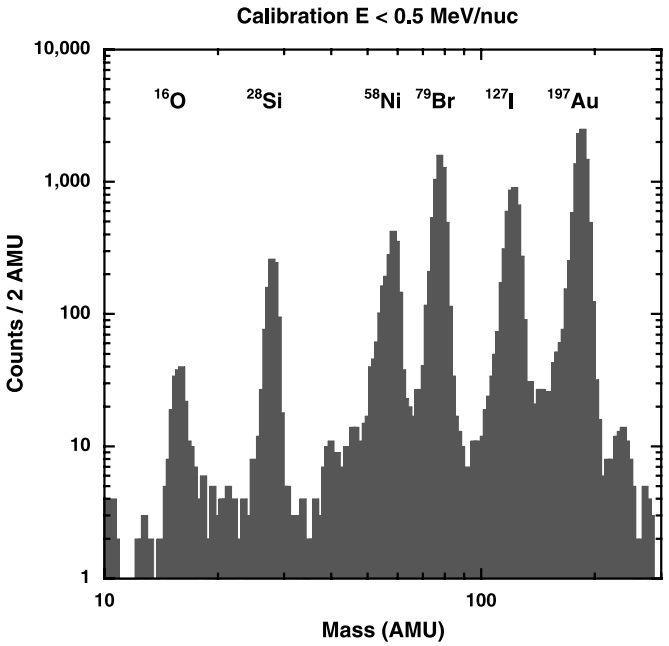

FIG. 1.—Mass peaks for selected heavy-ion species measured at less than 0.5 MeV nucleon^{-1} during an accelerator calibration with the ULEIS engineering model instrument. Note that the peaks are similar in width on the logarithmic mass scale, showing that σ_m/m is nearly constant for heavy ions.

In low count rate periods such as those emphasized here, we found that in the energy range above 0.5 MeV nucleon^{-1}, there were numerous inconsistent mass determinations for masses below $\sim$120 amu, so this region was excluded from the analysis below. For the remainder of the range we found that after removing events that had small microchannel-plate signals (typical of He nuclei), 11% $\pm$ 7% of the remaining events had inconsistent masses. We corrected for this relatively small background in the analysis below.

2.2. ^{3}He-*rich Event Selection*

Our previous studies of ^{3}He-rich SEP events have emphasized spectral forms, which require sampling over an extended energy range (Mason, Dwyer, & Mazur 2000; Mason et al. 2002b) and therefore require that magnetic connection to the flare site be maintained over a period of $\sim$24 hr or so. However, in many cases the ^{3}He-rich event is observed for only a portion of the time, with either the onset or decay phase interrupted or lost altogether (Mazur et al. 2000). For the present study, statistical accuracy in the measured abundances is emphasized, so we chose events that had easily observable ^{3}He enrichments and/or Fe/O enrichments of a factor of more than $\sim$3–4 (compared to large-SEP events) and a peak Fe intensity and duration sufficient to ensure good statistical accuracy for heavy-ion data. The threshold Fe intensity required depended on the length of the connection to the event and was in the range 0.1–0.3 particles/(s cm^2 sr MeV nucleon^{-1}). We examined particle velocity spectrograms (e.g., see Fig. 2 in Mason et al. 2002b) to ensure that the energy interval chosen for abundance measurements (320–450 keV nucleon^{-1}) was not interrupted by loss of magnetic connection to the event.

We surveyed the period 1997 September through 2003 April and found 20 events that met these criteria. Table 1 lists

TABLE 1

^{3}He-rich Solar Energetic Particle Event Properties

Number	Estimated Injection Time[a]	Onset[b]	Class[c]	^{3}He Fluence[d] ($\times 10^3$)	Fe Fluence[d] ($\times 10^3$)	^{3}He/^{4}He[d] ($\times 100$)	Fe/O[d]	$m > 100$/Fe[e] ($\times 10^3$)
1.....	1998 126.29	D	2	11.4 ± 1.1	38.0 ± 0.9	0.20 ± 0.09	1.01 ± 0.03	...
2.....	1998 136.06	S	2	0.33 ± 0.11	1.1 ± 0.1	0.49 ± 0.22	4.55 ± 0.61	4.2 ± 2.1
3[f].....	1998 148.34	S	1	44.4 ± 1.8	22.1 ± 0.6	2.63 ± 0.14	0.36 ± 0.01	...
4.....	1999 181.58	D	2	3.47 ± 0.30	5.8 ± 0.2	2.34 ± 0.26	2.31 ± 0.16	3.5 ± 1.1
5.....	1999 320.25	S	1	14.0 ± 1.4	9.8 ± 0.5	0.99 ± 0.18	0.53 ± 0.03	...
6.....	2000 092.83	D	1	5.14 ± 0.42	1.4 ± 0.1	13.6 ± 1.3	1.64 ± 0.19	4.7 ± 2.1
7.....	2000 118.63	D	2	19.8 ± 0.9	6.8 ± 0.2	1.16 ± 0.11	0.35 ± 0.01	<0.2
8[g].....	2000 122.42	D	1	5.71 ± 0.52	7.0 ± 0.3	5.52 ± 0.61	2.29 ± 0.16	1.8 ± 0.8
9.....	2000 145.0[h]	S	1	157.2 ± 4.0	22.2 ± 0.6	25.3 ± 0.8	2.03 ± 0.10	2.5 ± 0.7
10.....	2000 156.32	D	2	15.8 ± 0.8	8.5 ± 0.3	34.1 ± 1.3	1.49 ± 0.08	1.8 ± 0.7
11.....	2000 168.0[h]	D	2	11.7 ± 0.9	9.4 ± 0.3	1.09 ± 0.18	0.52 ± 0.02	...
12.....	2001 254.0[h]	S	2	6.6 ± 0.5	4.0 ± 0.2	6.89 ± 0.60	1.73 ± 0.12	0.9 ± 0.6
13.....	2001 345.59	D	2	37.7 ± 2.2	23.5 ± 1.0	0.54 ± 0.11	0.18 ± 0.01	...
14.....	2002 051.25	S	2	10.3 ± 0.6	20.2 ± 0.5	1.30 ± 0.13	1.73 ± 0.06	<0.14
15.....	2002 127.10	D	1	12.7 ± 0.8	3.1 ± 0.2	1.27 ± 0.15	0.25 ± 0.02	<0.5
16.....	2002 226.07	D	1	69.5 ± 4.0	77.2 ± 1.4	0.22 ± 0.08	0.38 ± 0.01	...
17.....	2002 232.11	D	1	51.6 ± 1.8	47.0 ± 0.7	1.99 ± 0.11	1.57 ± 0.04	0.6 ± 0.2
18.....	2002 266.03	D	2	24.9 ± 1.1	1.9 ± 0.2	40.5 ± 2.4	1.71 ± 0.21	<0.8
19.....	2003 012.66	S	2	4.6 ± 0.4	2.4 ± 0.1	9.12 ± 0.98	3.91 ± 0.48	2.3 ± 1.2
20.....	2003 118.25	D	1	11.8 ± 0.8	1.0 ± 0.1	8.1 ± 0.7	0.44 ± 0.06	<0.7

[a] Extrapolated injection time at Sun (year and decimal day of year).
[b] D = dispersive particle onset, S = spatial particle onset.
[c] ^{3}He-rich flare spectral classification (see text).
[d] From 320 to 450 keV nucleon^{-1}; fluence units are particles/(cm^2 sr MeV nucleon^{-1}).
[e] At 325 keV nucleon^{-1}; 1 count upper limits are used.
[f] Event 2 in Mason et al. 2000.
[g] Event 12 in Mason et al. 2000, 2002b; see also Kahler et al. 2001.
[h] Onset time has uncertainty of $\sim$0.5 days.

the events: the columns in the table are the estimated injection time at the Sun obtained by extrapolation of the particle data, the onset type (dispersive vs. ''spatial'' [nondispersive]), the spectral class (1 = power law or double power law, 2 = rounded Fe spectra), ^{3}He and Fe fluences, ^{3}He/^{4}He and Fe/O ratios, and the ratio of $m > 100$ amu nuclei to Fe. Ellipses in the $m > 100$/Fe ratio column are from events with count rates too high to measure UH abundances (see discussion below). Two events in the list have been included in earlier surveys.

Figure 2 shows the ratios of selected heavy elements to oxygen versus the Fe/C ratio for each of the 20 events in Table 1. This format follows the example of Reames, Meyer, & von Rosenvinge (1994, hereafter RMV) in choosing the Fe/C ratio for reference since at coronal temperatures C is nearly fully ionized, and therefore the enrichment of Fe is more clearly shown than if a less than fully stripped element such as O were used. In order to separate the data points in the figure, the ratios Ne/O, Mg/O, Si/O, S/O, Ca/O, and Fe/O have been multiplied by 10^{-X}, where $X = 1$, 2, 3, 3, 4, and 6, respectively. Squares with crosses and open diamonds respectively show averages for large-SEP events and impulsive-SEP events from the survey of Reames (1995). The N/O ratio is essentially independent of Fe/C, while the other ratios all increase with Fe/C, with the larger increases being associated with heavier elements. Although the correlations are fairly smooth, note that one event (number 18 in Table 1) has a much higher S/O ratio than would be expected from other abundances; this event is of an unusual type reported by Mason, Mazur, & Dwyer (2002a) wherein the heavy-ion enhancement pattern does not show a generally monotonic increase with mass. Only a few such events have been observed (see also Wiedenbeck et al. 2003a).

This generally smooth correlation of abundance enhancements seen in Figure 2 is similar to plots shown in the higher energy survey in RMV's Figure 8, with the present data having greatly improved statistical precision. However, RMV reported no significant correlation between the Fe/NeMgSi versus NeMgSi/CNO ratios. For the data in Figure 2, the correlation coefficient between Fe/NeMgSi and NeMgSi/CNO is 0.56, which for 20 points has only a $\sim$1% chance of being exceeded by a random population. While this difference with RMV might be due to spectral differences between the low energies surveyed here and the higher energy RMV survey (see Mason et al. 2000, 2002b), the fact that the overall average abundances between the two surveys agree well is evidence that spectra are not playing a critical role. Judging from the size of the statistical uncertainties shown in RMV, we suspect that the reason is that the RMV survey did not have the sensitivity to sample low values of Fe/NeMgSi and NeMgSi/CNO that are present in the current survey. In any case, the falling spectra of SEP events means that at the lower energies of the present survey we are more nearly able to sample the bulk of the particles than at high energies, and so in our discussion below we address the observed correlations shown in Figure 2.

Another interesting feature of Figure 2 is the distribution of events along the Fe/C axis: it is surprisingly uniform in $\ln(\mathrm{Fe}/\mathrm{C})$. One might expect that events with, e.g., Fe/C values on the low side of the distribution close to gradual events might be much more numerous, and on the high side quite rare. But this is not what is seen in the figure; rather, large Fe/C values are not dramatically less likely than others.

Figure 3 shows Fe/O and $m > 100$/Fe ratios from Table 1 versus Fe/C. Points where there were no counts above 100 amu,

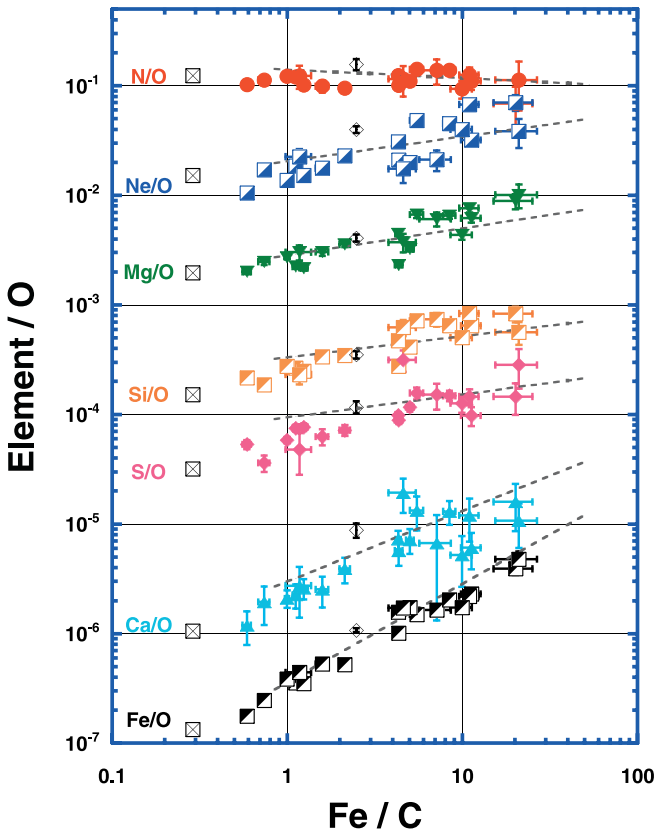

FIG. 2.—Ratios of heavy-ion elements to oxygen vs. the iron-to-carbon ratio for the 20 events in Table 1. *Squares with crosses*: Values from 5 to 12 MeV nucleon^{-1} in gradual solar particle events. *Open diamonds*: Impulsive-event ratios near 2.5 MeV nucleon^{-1} (both from the survey of Reames 1995). *Dashed lines*: Calculated variations described in text.

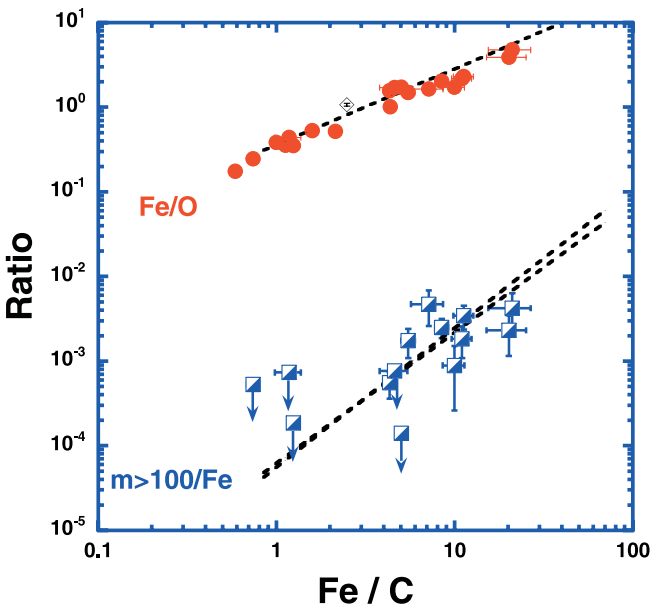

FIG. 3.—Same as Fig. 2, except for Fe/O and $m > 100$/Fe ratios. The two dashed lines through the $m > 100$/Fe points are calculated for two representative UH elements (Xe and Ba).

or just 1 count, are shown as 1 count upper limits in the figure. The open diamond is the survey average of Reames (1995) for impulsive events at ~2.5 MeV nucleon^{-1}. The data are consistent with $m > 100$/Fe increasing with Fe/C, but the uncertainties are large. Although limited by statistics for $m > 100$, note that the events with high $m > 100$/Fe are those that also have large Fe/C ratios even though these include some of the smaller events (e.g., events 2 and 6 in Table 1), so statistics alone do not appear to dominate the content of the figure. Figure 4 plots ^{3}He/^{4}He enhancements versus $m > 100$/Fe enhancements, where the reference populations used are slow solar wind (Gloeckler et al. 1999) and meteoritic abundances (Anders & Grevesse 1989), respectively. There is no evident correlation between the two enhancements, as has also been seen for ratios such as Fe/O versus ^{3}He/^{4}He (Mason et al. 1986; Reames et al. 1994). The enhancements of $m > 100$/Fe are generally as large or larger than the ^{3}He/^{4}He enhancement and reach values of ~1000 (see also Reames 2000).

2.3. *UH Spectra and Abundances*

In order to find more information about the UH spectra and abundances than is possible from the handful of counts in individual SEP events, we created a mission-long series of time intervals of "UH periods," making use of the fact that the UH nuclei are observed during impulsive-SEP events. To be included as a subinterval in this series, we required that the Fe/O ratio be greater than ~1 and that at least 1 count be observed above 70 amu for energies greater than 150 keV nucleon^{-1}. Thus a single subinterval would contain the time when the UH nucleus or nuclei came in, plus the time preceding or following that when Fe/O > ~1. In order to maintain proper normalization to the Fe peak, it was also necessary to require that the instrument event analysis rate be ≤6 events s^{-1}. Thus, only periods of low intensity, typical of impulsive-SEP events, were included. For the survey period from 1997 September through the end of 2003 April, there were 99 subintervals selected. The average period was 2.99 days in length, with the shortest being 7.2 hr and the longest 18.3 days. Many had only 1 or 2 UH counts. The summed observing time for the series was 295.7 days, which is 14.5% of the total time available for the survey. Considering that many lengthy periods of time were excluded by reason of high solar particle activity, it is clear that the UH periods were not at all unusual.

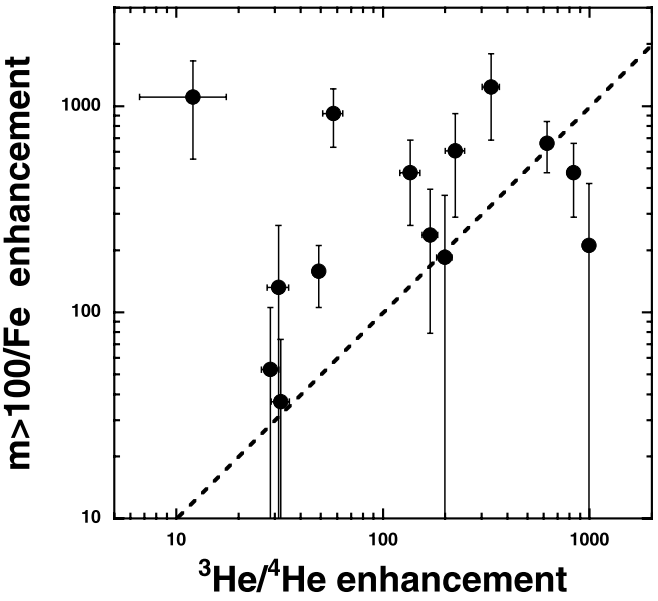

FIG. 4.—Enhancement factor of ^{3}He/^{4}He vs. $m > 100$/Fe. *Dashed line*: Location of 1:1 ratio.

Figure 5 shows spectra summed over the entire UH period for representative species, as well as UH mass groups 78–100, 125–150, and 180–200 amu. Notice in the figure that Fe/O ~ 1 over the entire energy range, as is typical of impulsive-SEP events, so it appears that the selection criteria did not bias the impulsive composition to any significant degree. The ^{3}He/^{4}He ratio is about 10%, highly enriched compared to the solar wind (e.g., Coplan et al. 1984). The spectra for the UH nuclei are similar to those for the lighter ions; this is consistent with the fact that the $m > 100$/Fe enrichments observed here are similar to those seen at significantly higher energies by Reames (2000).

Although the spectra shown in Figure 5 are plotted versus energy nucleon^{-1}, other possibilities exist. For example, Mason et al. (2002b) showed that in some ^{3}He-rich events the spectral forms of major species appeared to be more nearly of the same shape when plotted as functions of momentum charge^{-1} (rigidity). If we replot the data from Figure 5 as, e.g., functions of energy charge^{-1}, the heavy-nuclei abundances are further enhanced, but by a rather modest (factor of $\sim$2) amount since the spectra are not very steep. With such modest changes resulting in a change from MeV nucleon^{-1} to MeV charge^{-1}, it is not possible to state that one representation better organizes the data than the other. Since the relative abundance changes are small compared to the overall pattern observed, this question of energy nucleon^{-1} versus energy charge^{-1} spectral representation does not materially affect the discussion that follows.

Figure 6*a* shows the mass histogram for the UH period for the Fe peak and above. Figure 6*b* shows the same SEP data smoothed by five-bin running averages, along with solar system abundances. The solar system abundances use the table of Anders & Grevesse (1989), smeared out to be comparable to the ULEIS resolution in this region. This was done by spreading out each nuclide over adjacent mass bins using a Gaussian distribution and a mass resolution of $\sigma_m/m = 0.040$. Note that the broad peaks in the SEP data for the ranges 78–100, 125–150, and 180–220 amu are similar to features seen

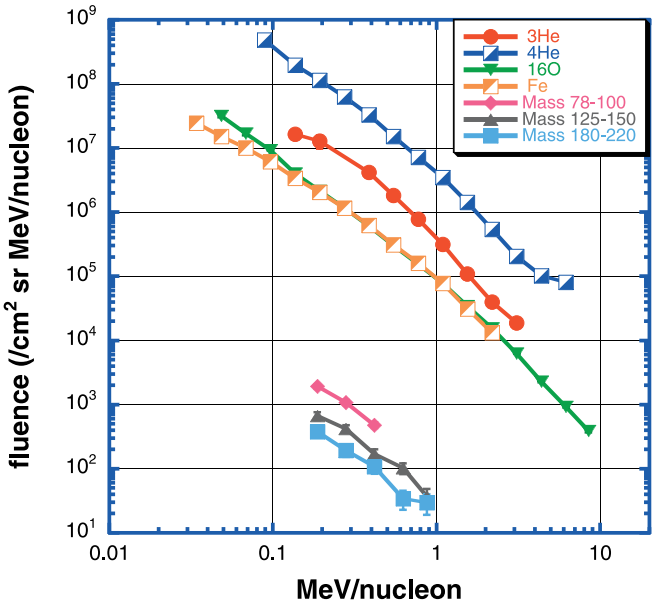

FIG. 5.—Energy spectra summed over all impulsive-event periods in which UH nuclei were observed.

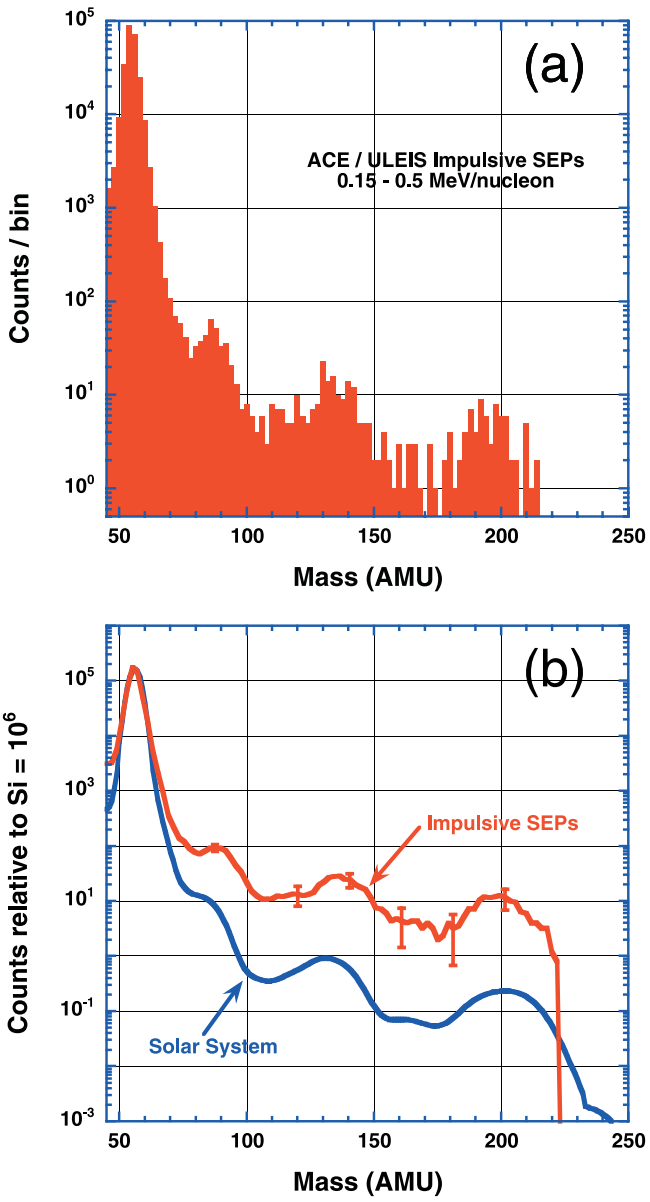

FIG. 6.—(*a*) Mass histogram of Fe peak and heavy nuclei during all periods in which UH nuclei were observed. (*b*) *Red curve*: Five-bin–smoothed data from (*a*) showing typical statistical uncertainties. *Blue curve*: Solar system abundances smoothed by mass resolution function of ULEIS (see text).

in the solar system abundances. Thus, even though there are no resolvable tracks in the in-flight ULEIS UH data, the presence of these features, along with a cutoff in events above $\sim$220 amu, provides a general confirmation of the mass calibration employed in the data analysis. In Figure 6*b* the SEP and solar system curves are normalized at the Fe peak and show increasing enhancements of SEP versus solar system material as mass increases.

Table 2 lists the UH-period SEP abundances normalized to O for individual elements in the range Fe and below, and for mass groups above that. The fourth column lists higher energy data from large, gradual SEP events (Reames 1995), and the fifth column lists the solar system abundances (Anders & Grevesse 1989) normalized to Fe. The sixth column shows the ratio of the ^{3}He-rich SEP abundances to the reference population, which is combined from the gradual SEP and

TABLE 2
^{3}He-rich Solar Energetic Particle Event Abundances

Species	Mass	^{3}He-rich SEP Abundance[a]	Gradual SEP Abundance[b]	Solar System Abundance[c]	^{3}He-rich SEP vs. Reference
^{4}He	4	54 ± 14[d]	57 ± 3	...	0.95 ± 0.24[d]
C	12	0.322 ± 0.003	0.465 ± 0.009	...	0.69 ± 0.01
N	14	0.129 ± 0.002	0.124 ± 0.003	...	1.04 ± 0.03
O	16	≡1.000 ± 0.006	≡1 ± 0.01	...	1.00 ± 0.01
Ne	20	0.261 ± 0.003	0.152 ± 0.004	...	1.72 ± 0.05
Mg	24	0.370 ± 0.003	0.196 ± 0.004	...	1.89 ± 0.04
Si	28	0.409 ± 0.004	0.152 ± 0.004	...	2.69 ± 0.07
S	32	0.118 ± 0.015	0.0318 ± 0.0007	...	3.70 ± 0.47
Ca	40	0.060 ± 0.003	0.0106 ± 0.0004	...	5.66 ± 0.38
Fe	56	0.950 ± 0.005[e]	0.134 ± 0.004	≡1	7.09 ± 0.21
	78–100	(9.6 ± 1.1)E−4	...	1.76E−4	40.7 ± 4.5
	125–150	(3.1 ± 0.6)E−4	...	1.95E−5	119.6 ± 23.0
	180–220	(2.2 ± 0.5)E−4	...	7.63E−6	215.4 ± 49.5

[a] 385 keV nucleon^{-1} (this work).
[b] 5–12 MeV nucleon^{-1} (Reames 1995).
[c] Meteoritic (Anders & Grevesse 1989).
[d] Uncertainty primarily due to instrumental efficiency (see discussion in Desai et al. 2003).
[e] Multiplied by a factor of 0.92 to correct for larger mass range summed in Fe group peak.

solar system values. We used Fe as the reference in the solar system abundances (rather than O) in order to approximately take account of the fact that most of the UH nuclei have a low first-ionization potential (FIP), while O has a high FIP (>∼10 eV) and this would inappropriately introduce an extra enhancement of ∼4.5 in the table (see discussion in Anders & Grevesse 1989). Figure 7 plots the enhancements from Table 2 and also shows the impulsive-SEP enhancements measured at higher energy in the Reames (1995) survey. Overall, the two data sets agree reasonably well. The Reames (2000) observations of UH nuclei in impulsive SEPs gave enrichments for $34 \leq Z \leq 40$ (∼79–91 amu) of ∼100 and for $50 \leq Z \leq 56$ (∼118–137 amu) of ∼1000; these are a bit larger than the values shown in Figure 7, but the rough size and trend for increase with mass are comparable.

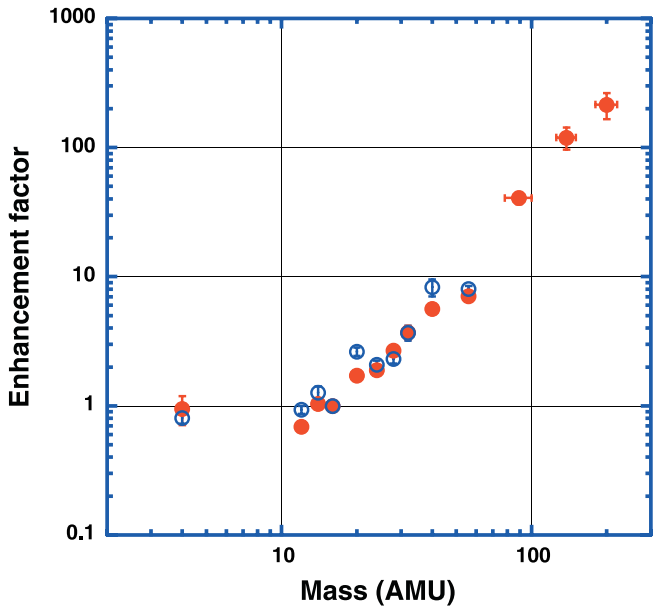

Fig. 7.—*Filled red circles*: Enhancement factor for ^{3}He-rich heavy-ion abundances, compared with gradual SEP ions and solar system abundances. *Blue circles*: Values from Reames (1995).

2.4. *Heavy-Ion Injection Times for the 2000 May 1 Event*

The small size of ^{3}He-rich SEP events, along with interplanetary scattering and frequent loss of magnetic connection, makes it difficult to derive injection times at the Sun. One event in this survey, number 8 in Table 1, is a notable exception. This event had the most nearly scatter-free propagation of any so far observed by ULEIS (see the spectrogram in Fig. 2 of Mason et al. 2002b) and was associated with a coronal mass ejection (CME) liftoff and X-ray event (see Kahler, Reames, & Sheeley 2001). The time-intensity profiles for heavy ions in this event were almost identical in shape and nearly symmetrical. By assuming a scatter-free flight path of 1.2 AU the major species all had virtually identical derived injection times over the energy range 90 keV nucleon^{-1} to 3 MeV nucleon^{-1}. Figure 8 (*top*) shows the injection time of Fe extrapolated back to the Sun, along with the *GOES* X-ray flux for this event; there is reasonably good coincidence between the Fe onset and the X-ray peak, which in turn coincided with the CME. The bottom panel of Figure 8 shows deviations of the injection times around the average value for all species: the deviations are shown since they are less sensitive to uncertainties in the interplanetary magnetic field path length. Note that for the ^{3}He and major species, the injections all appear to be simultaneous and that, with larger uncertainty, UH nuclei were also injected simultaneously with the others. In addition, 38–315 keV electrons in this event were also released simultaneously with the heavy ions (Mewaldt et al. 2003).

2.5. *Summary of Observations*

The main observational features found in our survey are as follows:

1. Relative to O, heavy ions through Fe are enriched in ^{3}He-rich SEP events, with the enrichments increasing with increasing mass number.
2. The heavy-ion enrichments are well correlated, e.g., events with larger Fe/C ratios also show larger enrichments in other heavy ions.
3. Heavy-ion enhancements are roughly uniformly distributed in Fe/C enhancement: there is no strong preference for events in one part of the observed distribution.

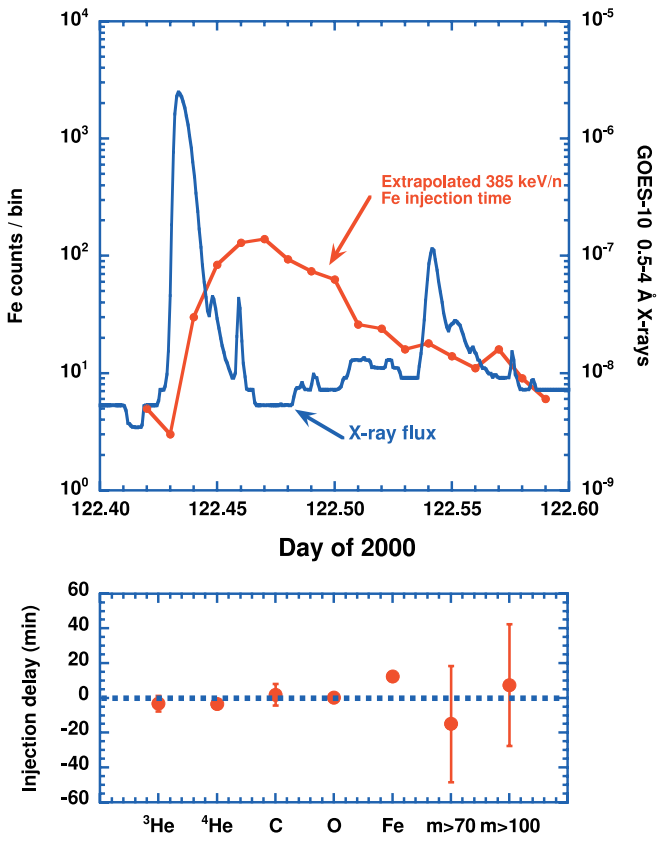

FIG. 8.—*Top*: Extrapolated injection time for Fe nuclei in the event of 2000 May 1, and *GOES 10* 0.5–4 Å X-rays. *Bottom*: Deviation of mean injection times for ^{3}He, major species, and UH nuclei from the average injection time of all species.

4. UH nuclei are commonly seen in ^{3}He-rich events, and their abundance positively correlates with Fe/C.

5. UH spectra measured from ~0.1–1 MeV nucleon^{-1} have shapes similar to those of major species such as He, O, and Fe.

6. The distribution of mass groups of UH nuclei shows broad peaks similar to those in compilations of solar system abundances.

7. Relative to O, the enhancement of heavy nuclei increases with mass, reaching average values of ~7 for Fe, ~40 for mass 78–100 amu, ~120 for mass 125–150 amu, and ~215 for 180–220 amu.

8. Compared to meteoritic material, the enhancements of $m > 100$/Fe reach values of ~1000 in individual SEP events and are generally larger than the ^{3}He/^{4}He enhancements in the same event.

9. Average injection times in one especially clean event were within ±6.4 minutes of each other for major species and ^{3}He and within ~15 minutes for UH nuclei; i.e., they all appear to be simultaneously injected.

3. DISCUSSION

3.1. *Dependence on Charge-to-Mass Ratio*

Since SEP acceleration and transport are believed to depend on particle *Q/M* ratio, discussions of heavy-ion abundance observations often discuss the data using this variable (e.g., Breneman & Stone 1985; Reames et al. 1994; Cohen et al. 1999). It has been long known that ^{3}He-rich event energetic particle charge states show a high degree of ionization, with elements up through Si essentially fully stripped (Klecker et al. 1984; Luhn et al. 1987). This poses a dilemma since if Si has the same *Q/M* ratio as, e.g., O, then it appears impossible to construct an acceleration mechanism that will yield, e.g., the enhanced Ne, Mg, and Si/O ratios observed in ^{3}He-rich events (e.g., Luhn et al. 1987). A possible resolution to this problem is that the energetic particles are stripped after the acceleration mechanism has enhanced them, as discussed by RMV. More recent observations of Fe charge states in ^{3}He-rich events have also been interpreted as evidence of stripping since the new results show a strong energy dependence wherein the high charge states observed by Luhn near 0.5 MeV nucleon^{-1} have been observed to decrease dramatically toward lower energies (Möbius et al. 2003). We therefore have a situation where it is not clear what charge-state values to use in discussing the present data; in fact, if the particle charge states change during the acceleration process, it may not be meaningful to use single average *Q* values for each element.

In Figure 9 we explore these issues by plotting the enhancement factors from Table 2 with respect to particle *Q/M* ratio for some representative charge states. In the figure, the red points are based on calculated equilibrium charge states in a 3.2 MK plasma; for Fe and lighter elements, we use the tables of Arnaud & Rothenflug (1985) and Arnaud & Raymond (1992); for heavier elements we use the tables of Post et al. (1977). Other points in the figure are as follows: blue circles use the large-SEP charge states from Luhn et al. (1985), the inverted blue triangle shows the location of Fe if one uses the lower Fe charge state observed in the large-SEP event in 1992 (Mason et al. 1995), and the dashed line shows the range of Fe *Q/M* values from the Möbius et al. (2003) survey of impulsive events. (If we were to show the points plotted with the high average impulsive-flare charge states from Luhn, they would

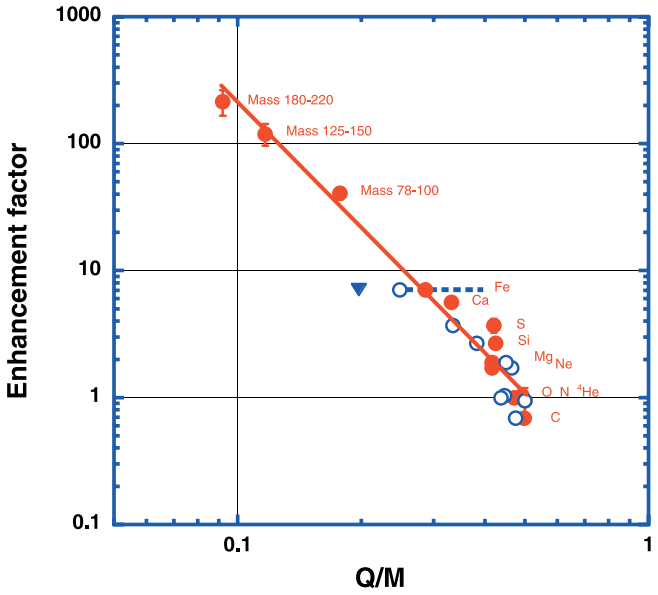

FIG. 9.—Abundance enhancement factor for impulsive-event survey vs. *Q/M* ratio, using charge state from calculations of a 3.2 MK equilibrium plasma (*red filled circles*), direct measurements of energetic particles in three large solar particle events (*blue circles*), direct measurements of Fe ionization state in the 1972 November large-particle event (*blue inverted triangle*), and a range of Fe ionization states observed in several impulsive solar particle events (*dashed line*). The solid line is a power-law fit to the red points and has a slope of −3.26.

all fall near $Q/M \sim 0.5$.) Since stripping increases the charge states, Möbius et al. (2003) concluded that the lowest charge states that they observed (corresponding to their lowest energy measurements) put an upper limit on the initial ionization state of the plasma. Thus, Möbius et al. (2003) conclude that in the figure, the Fe points at high Q/M values reflect stripping, while those at lower values may approach the initial plasma. For Fe, this is close to the charge state observed by Luhn in large, gradual particle events.

Although the figure shows a general organization of the data by Q/M, the correlations do not fall neatly along a single line, and given the event-to-event and energy variations in charge state seen by Möbius et al. (2003) in impulsive events, it appears that no single value of Q/M exists for Fe or presumably for other partially stripped heavy nuclei. For the UH nuclei of interest here, there are only the calculated charge states available, and these are used in the figure. Also shown is a power-law $(Q/M)^{\gamma}$ fit to the data points using the calculated charge states; it has a slope $\gamma = -3.26$. Si and S show the largest deviations from this fit, but given the other variations shown, e.g., by Fe, it is hard to assess the significance of this.

In order to explore the heavy and UH abundance variations further, we use calculated charge states, since only they are available for selected UH nuclei and they can also be related to ambient temperatures that could be relevant in identifying source conditions. Figure 10 shows calculated mean equilibrium Q/M ratios of selected elements over a broad temperature range that is typical of various regions of the corona and coronal loops. In the figure, elements of similar mass and enhancement values are shown in the same color; the solid lines are for high-FIP elements (>10 eV) and the dashed lines are for low-FIP elements. It is immediately apparent that the UH nuclei open up an entirely new range of Q/M ratios where enhancements are present. Note that we have shown only a few representative UH nuclei on this figure; if all were shown the lower part of the figure would be nearly filled with lines.

We can explore the enhancement factors as a function of temperature using the power law $(Q/M)^{\gamma}$ shown in Figure 9

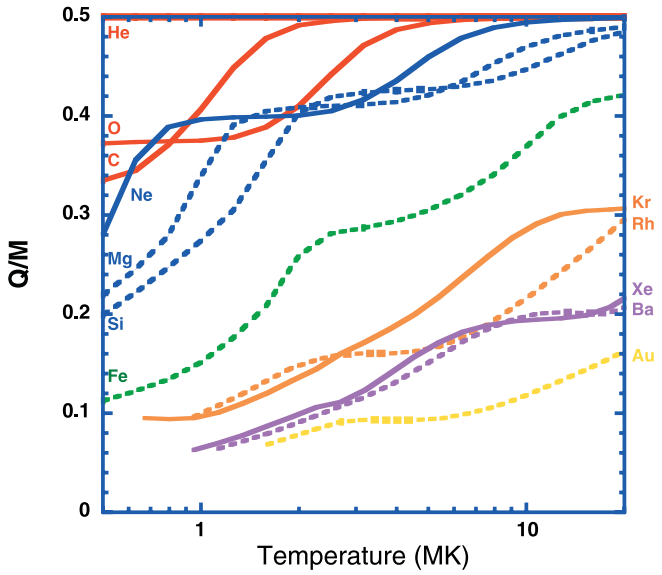

FIG. 10.—Calculated equilibrium Q/M ratios for selected elements. Elements with the same color have similar enhancements. *Solid lines*: High-FIP elements. *Dashed lines*: Low-FIP elements.

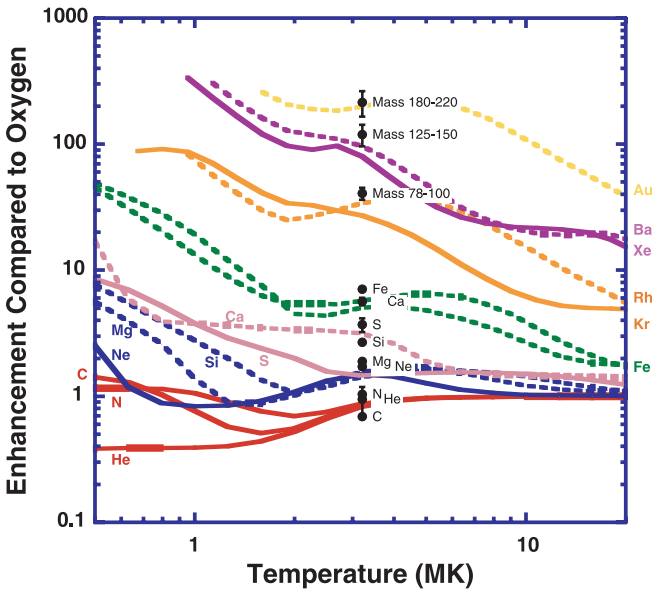

FIG. 11.—Calculated enhancement factors relative to O for selected elements. Observed enhancements (*black symbols*) are from Table 2 and arbitrarily plotted at 3.2 MK.

and a reference element such as O (e.g., see Cohen et al. 1999). Using the power-law exponent from the fit in Figure 9, the enhancement factor F for element X compared to O is $F = [(Q/M)_X/(Q/M)_O]^{-3.26}$, where values of Q for each temperature are obtained from the calculations cited above. Figure 11 shows F over a range of temperatures. The observed enhancements from Table 2 are plotted arbitrarily at 3.2 MK, a temperature often used in discussions of ^{3}He-rich flares since it is in a range where Ne, Mg, and Si have Q/M ratios different from those of O, which could be required to explain their enhancement (e.g., RMV; see also the discussion of active region temperatures in Appendix A of Steinacker et al. 1997). The agreement between the calculated enhancements and observed values is reasonably good, with Si and Ca showing the largest deviations (factor of ~1.7) from the curves. Note that the predicted enhancements are comparable in size over a sizeable temperature range, from ~2.5 to ~6 MK. In addition, the enhancement for Si and heavier elements are also compatible with quiet-loop temperatures closer to 1–1.4 MK (e.g., Feldman, Widing, & Warren 1999), but those for Ne and Mg are not. (The two lines for Fe use the Arnaud & Raymond 1992 and the Post et al. 1977 values separately in order to illustrate the sensitivity of the calculation to the differences between the two tables of calculated charge states.)

The power-law index γ in (Q/M) variation is known to vary from one large-SEP event to another (e.g., Mewaldt & Stone 1989; Leske et al. 1999). Figure 12 explores this variation for the Ne/O versus Fe/C ratio for the ^{3}He-rich events studied here (*red filled circles*), as well as for large-SEP events observed at 3.5–50 MeV nucleon^{-1} on *Voyager* (Breneman 1985). The observed variation of Ne/O implies a range of roughly $5 > \gamma > -12$ (see also Cohen et al. 1999; Leske et al. 1999). Note that several points from the two sets of data overlap each other, even though one is from high energies and intense SEP events and the other from low energies and ^{3}He-rich events. The dashed line in the figure is only a rough fit to the data: although possibly consistent with the data points with lower Fe/C values (which have very sizeable uncertainties), it seems to systematically underestimate the steepness of the increase

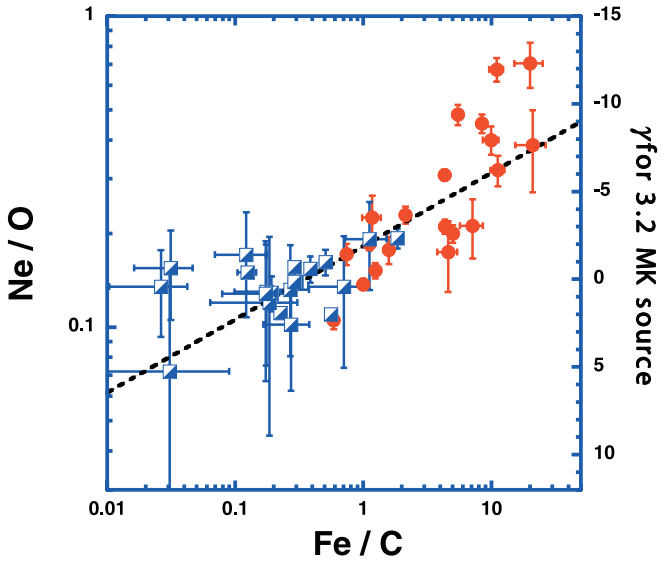

FIG. 12.—Ne/O vs. Fe/C for this work (*red filled circles*) at 375 keV nucleon^{-1} ^{3}He-rich events, and for 3.5–50 MeV nucleon^{-1} large-SEP events from Breneman (1985; *half-filled blue squares*). The black dashed line and right axis show power-law exponent γ associated with points along the line assuming ionization states at 3.2 MK (note reversed scale).

of Ne/O at high values of Fe/C. The dashed lines shown in Figures 2 and 3 were also calculated using the power law in *(Q/M)*, normalized to the Table 2 abundances for $\gamma = -3.26$. They give a rough fit to the data, but in addition to Ne, elements such as Si and S appear to have stronger dependence on Fe/C than given by the power law.

3.2. *Implications for Acceleration Models*

We now discuss the implications of these new observations in the context of previous work. The clear association of ^{3}He enrichment with enrichment of heavy nuclei has long been a key property addressed in theoretical models of these events. An early work in this area (Fisk 1978) proposed a model of resonant plasma heating of ^{3}He and noted that partially stripped heavy nuclei might also be preferentially heated since their *Q/M* ratio was near the favored range. The Fisk (1978) model assumed a second stage of acceleration after this preferential heating. For the UH nuclei enhancements reported here, however, the Fisk mechanism apparently has significant problems. First, the *Q/M* ratios of the UH nuclei are far from the required values for favorable heating. Second, instead of being modest, the UH enrichments usually exceed the ^{3}He/^{4}He enrichment itself. So to incorporate the UH enrichment into a model of this kind requires additional complexity and assumptions about, e.g., heating. All this would serve to make the model dependent on increasingly special conditions, yet we have seen that SEP events with UH enhancements are common, making any specialized set of model conditions unattractive. We conclude that the very large and commonly observed UH abundance enhancements reported here do not appear to be easily accommodated by this model, while emphasizing that the special heating of ^{3}He may be due to this mechanism.

In addition to the Fisk mechanism, there have been a number of other plasma heating processes proposed (e.g., Temerin & Roth 1992; Zhang 1995, 1999). It is not clear to what extent these observed properties of UH enhancements can be accommodated by these models.

Another theoretical approach has built on the observed fact that the ^{3}He/^{4}He enrichment is not correlated with the Fe/O enrichment (Mason et al. 1986), and uses cascading MHD turbulence to accelerate nuclei and produce enrichments in the range Ne–Fe (Miller 1998). This stochastic model is able to reproduce observed features of the particle spectra as well as the heavy-nuclei enhancements for Ne–Fe (Mason et al. 2002b). This process does not enrich ^{3}He, and so that enhancement requires a distinct, separate mechanism (Miller 1998). However, the cascading MHD turbulence model of Miller (1998) does not easily lead to UH enhancements of the kind that we observe, since in this model the degree of enrichment arises from the energy available to heat the ions. In this process, Fe ions are heated before Ne, Mg, and Si, and because the Fe absorbs a significant portion of the wave energy, the Ne, Mg, and Si ions are less strongly heated and therefore show a smaller enhancement (see discussion in Mason et al. 2002b). Although UH nuclei could easily be heated in this model, their extremely low abundance means that they could not absorb significant energy and so their enhancement would be predicted to be the same as Fe (J. A. Miller 2003, private communication), and this would be inconsistent with the observations presented here.

The heavy-ion data presented here suggest a mechanism in which abundance enhancements are related to the *Q/M* ratio of the ion. A number of mechanisms, including betatron acceleration or shock-surfing, might produce such enhancement. In particular, preferential acceleration of heavy ions is a feature in models of "smoothed" shocks, i.e., shocks where the plasma velocity jump at the shock takes place over a scale of the distance of the particle diffusion length. In this situation, heavy ions with their larger gyroradii have larger upstream diffusion lengths than lighter ions. They therefore experience a larger effective compression ratio, resulting in acceleration increasing uniformly with *Q/M* (e.g., Eichler 1979; Ellison, Jones, & Eichler 1981; Pesses, Jokipii, & Eichler 1981; Ellison 1985; Ellison & Möbius 1987; Ellison, Baring, & Jones 1995; Jokipii & Giacalone 1996; Ellison, Drury, & Meyer 1997; Ellison, Jones, & Baring 1999). Diffusive-compressive acceleration (Giacalone, Jokipii, & Kóta 2002) is an extreme example of this kind of phenomenon. There are competing effects that may decrease this enhancement. For example, the acceleration rates for heavy ions may be slower than for light ions since their gyrofrequencies are lower; in addition, if particles leave the shock acceleration region by propagating a certain distance upstream, the larger gyroradius particles may escape first. Thus, either a steady state mechanism is required to preserve the enhancement (Ellison et al. 1997), or escape from the shock must occur in a manner that does not select out the high-rigidity particles (e.g., Eichler 1981; Lee 1982). As is the case for stochastic models such as Miller's, a separate mechanism would be required to enrich the ^{3}He.

4. SUMMARY AND CONCLUSIONS

We have surveyed the heavy and UH composition in ^{3}He-rich SEP events and have found that when compared to reference solar corona or meteoritic abundances, these events show Fe/O enhanced by $\sim$10 and heavier elements up to the range 180–220 amu enhanced by an additional factor of $\sim$100. The enhancements of major elements in the range Ne–Fe are all well correlated, with the largest enhancements being for Fe. The UH-element (mass 78–220 amu) enrichments are positively correlated with the Fe enrichment and are much

larger. We find that UH nuclei are commonly present in these ^{3}He-rich events. Since ^{3}He-rich events occur frequently, the underlying physical mechanisms must be widely present in the acceleration region.

The average abundances and flare-to-flare abundance variations can be organized approximately as a power law in the *Q/M* ratio and fit smoothly onto previously published heavy-ion elemental abundance variations in large, shock-associated SEP events. This smooth joining of the large-SEP and ^{3}He-rich SEP abundance variations may suggest that these two ''types'' of events may not in fact be distinct and that their acceleration mechanisms have more in common than is generally assumed. Further investigation into both stochastic and shock acceleration processes will be required to determine whether they can explain the features reported here.

We thank the many individuals at the University of Maryland and the Johns Hopkins Applied Physics Laboratory for the construction of the ULEIS instrument. We thank S. Krucker, R. P. Lin, J. A. Miller, and G. Gloeckler for illuminating discussions. The X-ray data in Figure 8 were obtained from the *GOES* World Wide Web site. This work was supported in part by NASA under Caltech grant 44A1055749 at the University of Maryland.

REFERENCES

Anders, E., & Grevesse, N. 1989, Geochim. Cosmochim. Acta, 53, 197
Arnaud, M., & Raymond, J. 1992, ApJ, 398, 394
Arnaud, M., & Rothenflug, R. 1985, A&AS, 60, 425
Breneman, H. H. 1985, Ph.D. thesis, Caltech
Breneman, H. H., & Stone, E. C. 1985, ApJ, 299, L57
Cohen, C. M. S., et al. 1999, Geophys. Res. Lett., 26, 149
Coplan, M. A., Ogilvie, K. W., Boschler, P., & Geiss, J. 1984, Sol. Phys., 93, 415
Desai, M. I., et al. 2003, ApJ, 588, 1149
Dwyer, J. R., Mason, G. M., Mazur, J. E., Gold, R. E., Krimigis, S. M., Möbius, E., & Popecki, M. 2001, ApJ, 563, 403
Eichler, D. 1979, ApJ, 229, 419
———. 1981, ApJ, 244, 711
Ellison, D. C. 1985, J. Geophys. Res., 90, 29
Ellison, D. C., Baring, M. G., & Jones, F. C. 1995, ApJ, 453, 873
Ellison, D. C., Drury, L. O. C., & Meyer, J.-P. 1997, ApJ, 487, 197
Ellison, D. C., Jones, F. C., & Baring, M. G. 1999, ApJ, 512, 403
Ellison, D. C., Jones, F. C., & Eichler, D. 1981, J. Geophys. Res., 50, 110
Ellison, D. C., & Möbius, E. 1987, ApJ, 318, 474
Feldman, U., Widing, K. G., & Warren, H. P. 1999, ApJ, 522, 1133
Fisk, L. A. 1978, ApJ, 224, 1048
Giacalone, J., Jokipii, J. R., & Kóta, J. 2002, ApJ, 573, 845
Gloeckler, G., et al. 1999, Geophys. Res. Lett., 26, 157
Jokipii, J. R., & Giacalone, J. 1996, Space Sci. Rev., 78, 137
Kahler, S. W., Reames, D. V., & Sheeley, N. R., Jr. 2001, ApJ, 562, 558
Klecker, B., Hovestadt, D., Gloeckler, G., Ipavich, F. M., Scholer, M., Fan, C. Y., & Fisk, L. A. 1984, ApJ, 281, 458
Kocharov, L. G., & Kocharov, G. E. 1984, Space Sci. Rev., 38, 89
Lee, M. A. 1982, J. Geophys. Res., 87, 5063
Leske, R. A., Mewaldt, R. A., Cohen, C. M. S., Cummings, A. C., Wiedenbeck, M. E., Christian, E. R., & von Rosenvinge, T. T. 1999, Geophys. Res. Lett., 17, 2693
Luhn, A., Klecker, B., Hovestadt, D., & Möbius, E. 1987, ApJ, 317, 951
Luhn, A., et al. 1985, in Proc. 19th Int. Cosmic Ray Conf. (La Jolla), 4, 241
Mason, G. M., Dwyer, J. R., & Mazur, J. E. 2000, ApJ, 545, L157
Mason, G. M., Mazur, J. E., & Dwyer, J. R. 1999, ApJ, 525, L133
———. 2002a, ApJ, 565, L51
Mason, G. M., Mazur, J. E., Looper, M. D., & Mewaldt, R. A. 1995, ApJ, 452, 901
Mason, G. M., Reames, D. V., Klecker, B., Hovestadt, D., & von Rosenvinge, T. T. 1986, ApJ, 303, 849
Mason, G. M., et al. 1998, Space Sci. Rev., 86, 409
———. 2002b, ApJ, 574, 1039
Mazur, J. E., Mason, G. M., Dwyer, J. R., Giacalone, J., Jokipii, J. R., & Stone, E. C. 2000, ApJ, 532, L79
Mewaldt, R. A., & Stone, E. C. 1989, ApJ, 337, 959
Mewaldt, R. A., et al. 2003, in Proc. 28th Int. Cosmic Ray Conf. (Tsukuba), 6, 3313
Miller, J. A. 1998, Space Sci. Rev., 86, 79
Möbius, E., Cao, Y., Popecki, M., Kistler, L. M., Kucharek, H., Morris, D., & Klecker, B. 2003, in Proc. 28th Int. Cosmic Ray Conf. (Tsukuba), 6, 3273
Pesses, M. E., Jokipii, J. R., & Eichler, D. 1981, ApJ, 246, L85
Post, D. E., Jensen, R. V., Tarter, C. B., Grasberger, W. H., & Lokke, W. A. 1977, At. Data Nucl. Data Tables, 20, 397
Price, P. B., Chan, J. H., Hutcheon, I. D., MacDougall, D., Rajan, R. S., Shirk, E. K., & Sullivan, J. D. 1973, Geochim. Cosmochim. Acta, 3 (Suppl. 4), 2347
Reames, D. V. 1995, Adv. Space Res., 15(7), 41
———. 1999, Space Sci. Rev., 90, 413
———. 2000, ApJ, 540, L111
Reames, D. V., Meyer, J. P., & von Rosenvinge, T. T. 1994, ApJS, 90, 649 (RMV)
Shirk, E. K., & Price, P. B. 1973, in Proc. 13th Int. Cosmic Ray Conf. (Denver), 2, 1474
Steinacker, J., Meyer, J.-P., Steinacker, A., & Reames, D. V. 1997, ApJ, 476, 403
Stone, E. C., Frandsen, A. M., Mewaldt, R. A., Christian, E. R., Margolies, D., Ormes, J. F., & Snow, F. 1998, Space Sci. Rev., 86, 1
Temerin, M., & Roth, I. 1992, ApJ, 391, L105
Wiedenbeck, M. E., Leske, R. A., Cohen, C. M. S., Cummings, A. C., Mewaldt, R. A., Stone, E. C., & von Rosenvinge, T. T. 2003a, in Proc. 28th Int. Cosmic Ray Conf. (Tsukuba), 6, 3245
Wiedenbeck, M. E., et al. 2003b, in AIP Conf. Proc. 679, Solar Wind Ten, ed. M. Velli, R. Bruno, & F. Malara (Melville: AIP), 652
Zhang, T. X. 1995, ApJ, 449, 916
———. 1999, ApJ, 518, 954